C. R. Mecanique 338 (2010) 556–569

Contents lists available at ScienceDirect

Comptes Rendus Mecanique

www.sciencedirect.com

Micromechanics of granular materials

Evolution of functional connectivity in contact and force chain networks: Feature vectors, *k*-cores and minimal cycles

Évolution de connectivité fonctionnelle des réseaux de contact et de chaines de force

Antoinette Tordesillas *, Patrick O'Sullivan, David M. Walker, Paramitha

Department of Mathematics & Statistics, University of Melbourne, Parkville, Victoria 3010, Australia

ARTICLE INFO

Article history:
Available online 20 October 2010

Keywords:
Rheology
Granular materials

Mots-clés :
Rhéologie
Matériaux granulaires

ABSTRACT

We analyze the rheological response, i.e., fabric and contact force evolution, of dense granular materials from a complex networks perspective. The strain evolution of three classes of subnetworks, i.e., *k*-cores, minimal cycles and force chain networks, elucidates the breakdown of functional connectivity and structure in the lead up to and during failure. Feature vectors and dynamics occurring in such networks in three different biaxially compressed two-dimensional samples reveal some common aspects which are suggestive of an intrinsic structural hierarchy in granular networks – while differences shed light on the influence of confining pressure and interparticle rolling resistance on the evolution of these networks both at the mesoscopic as well as macroscopic levels.

RÉSUMÉ

Nous analysons la réponse constitutive de matériaux granulaires denses, au travers de l'évolution des forces de contact et de la texture, dans le cadre des réseaux complexes. L'évolution des déformations de trois classes de sous-réseaux, comprenant les cycles minimaux et les chaines de force, permet d'éclairer la disparition de connectivité fonctionnelle et de structure au cours du processus de rupture. L'analyse des processus dynamiques associés à de tels réseaux, au sein d'échantillons comprimés de manière biaxiale, révèle des aspects communs qui suggèrent l'existence d'une hiérarchie structurelle intrinsèque. En outre, l'influence de la pression de confinement et de la résistance au roulement inter-particulaire sur l'évolution de tels réseaux apparaît clairement aux échelles mésoscopique et macroscopique.

1. Introduction

The last few decades have witnessed significant developments in fundamental geomechanics, with much of the impetus arguably emanating from micromechanics – in particular, those from computer simulations using the discrete element method (DEM): see, for example, [1–11]. Unquestionably, the widespread appeal of DEM resides in its capability to not only handle large-scale problems, but also deliver a wealth of information across multiple length scales, from the particle scale to

* Corresponding author.
E-mail address: atordesi@ms.unimelb.edu.au (A. Tordesillas).

1631-0721/$ – see front matter
doi:10.1016/j.crme.2010.09.004

the bulk. Such benefits come at a price: large scale problems require prohibitive amounts of CPU time and DEM simulations invariably generate large volumes of data. This article will be focused on the latter problem of analysis. These data must be somehow processed and analyzed efficiently, and then interpreted, before new insights into the granular structure and rheological behaviour can be finally established. Turning data into knowledge is, of course, much easier said than done. Consequently, a key challenge confronting future DEM-based explorations into granular behaviour is the development of methods that can mine useful information from such simulations, effectively and efficiently.

In DEM simulations, as originally introduced in the seminal paper of [11], the mechanical response of a geomaterial (e.g., soil or rock mass) is governed by the interactions at the contacts between constituent particles and between particles and the boundaries. These interactions have long been recognized to be those responsible for the emergent complexity observed in these materials [12,13]. Herein, we present relatively new techniques not only in soil micromechanics but, more broadly, in DEM studies of granular materials, wherein the contact interactions are analyzed from the perspective of networks. These interactions are ultimately defined by not just the (a) topology (fabric) of the contact network and (b) the spatial distribution of the contact forces and moments at a given strain state – but also by the co-evolution of both of these throughout loading history. The aim of this study is to quantitatively characterize this co-evolution using relatively nascent techniques to deliver new insights on granular rheology, with attention paid to the effects of confining pressure and rolling resistance used in DEM models to account for particle shape [14].

Networks underpin virtually all of complex systems. Indeed in one of the most favoured paradigms of complexity, i.e., the broad class of dense and cohesionless granular materials that embodies many types of geomaterials, numerous types of networks can be conceived. Depending on the type of network, various aspects of functional activity and rheological behaviour can be uncovered. Perhaps the most obvious networks in granular materials that naturally lend themselves to a complex network analysis are the contact and contact force networks, although very few have examined these formally using the theory of complex networks (e.g., [15–19]).

Complex networks offer numerous statistical measures for large graphs thus making it ideal for the study of networks emerging in quasistatically deforming dense granular materials; [20–25] and references cited therein provide some background in this intensely active area of research. Preliminary studies show that techniques from this discipline can potentially crystallize understanding of granular systems, especially when overlaid with information on material behaviour derived from other disciplines, e.g., structural stability from structural mechanics and invariant dynamics from dynamical systems theory [19,26–28].

Complex networks also offer methods whereby fabric and force anisotropy can be studied separately or jointly. The topology of each contact network, e.g., distributions of inter-particle contacts, distributions of cycles and local density of 3-cycle configurations, all summarized succinctly through various complex network measures can probe the fabric anisotropy of the material. The network analysis can go further and capture force anisotropy through consideration of weighted networks. In this case, each link in the contact network topology can be assigned a weighting related to the contact force and weighted analogues of the network measures probing fabric (e.g., strength, subgraph intensity and coherence [29]) can help to reveal detail about fabric and force anisotropy.

In this investigation, we explore bulk as well as mesoscopic patterns of behaviour and dynamics in the networks of three distinct two-dimensional polydisperse assemblies of cohesionless circular particles. The samples are subject to biaxial compression, with two of the samples deforming under constant confining pressure, while the third is under constant volume and varying confining pressure. We exploit the differences in these samples to probe the effect of rolling resistance and boundary conditions on functional connectivity. In particular, we seek to characterize the evolution of functional connectivity from three aspects of complex networks: feature vectors, minimal cycles and k-cores. To the best of our knowledge, this constitutes the first study undertaken to probe the effects of material parameters and boundary conditions on granular rheology using this blend of techniques from complex networks.

Before proceeding, it is useful at this juncture to gain some insights into the motivation for this study and rationale for the particular choice of techniques used in the ensuing analysis. The main inspiration stems from preliminary evidence from numerical simulations and experiments on photoelastic disks, which suggests that a dense granular material forms distinct structures out of modular building blocks, e.g., force chains and 3-cycles, during deformation [19,26–28,30]. Photoelastic disk experiments and numerical simulations have shown force chains, i.e., quasi-linear chains of particles form in the direction of major (most compressive) principal stress, and serve the most important function in a material under load: that is, they act as primary load bearers by transmitting the majority of the load applied to the assembly [31–33]. The 3-cycles, formed by three particles in mutual contact, can be likened to trusses while the force chains can be likened to the strong columns in man-made architectural structures [26]. Connections between force chain particles and 3-cycles are therefore of chief importance to force transmission. Moreover, the breakdown of these functional connections holds vital consequences for the stability and thus load-carrying capacity of granular materials. These observations prompt some obvious questions. How do connections between particles in such granular structures evolve? What new insights on granular rheology can we uncover from a quantitative analysis of the evolution of these connections?

Feature vectors exemplified here summarize the evolution of degree, clustering coefficient, subgraph centrality and network bipartivity [22,23,25]. We focus on these network features since these quantify the minimal cycle membership that a given particle is part of. Minimal cycles, which are the shortest closed self-avoiding walks in a network or graph, are important to force chains from at least two perspectives [26]. Odd-cycles (e.g., 3-cycles, 5-cycles etc.) frustrate relative rotations. Consequently, odd-cycles serve as key stabilizing agents since relative rotations are a major contributor to the mobilization

or failure of contacts in granular systems. By contrast, even-cycles (e.g., 4-cycles, 6-cycles etc.) allow particles to rotate freely. This distinction holds important ramifications for force chain stability.

Specifically, the key mechanism for failure of force chains, i.e., buckling, is governed by relative particle rotations. As recently shown in [26], the presence of 3-cycles around force chains prolongs the lifetime of force chains, especially if these cycles transmit relatively large forces at their contacts. Indeed, this prompted the introduction of the concept of 3-force cycles, i.e., strong 3-cycles where each contact bears above-the-global average force magnitude [26]. 3-force cycles stabilize force chains by providing dual resistance to buckling – first, by frustrating rotations and, second, by providing strong lateral support. Interestingly, we have also found that n-force cycles exhibit a different frequency distribution than the general n-cycle membership which may suggest a subtle difference in their role within the evolving network of a deforming granular material.

Minimal cycles, in general, are also useful in characterizing deformation: for example, local dilatation may be viewed as a process by which adjacent small 3/4-cycles open up and combine to form a large n-cycle ($n \geqslant 5$) encircling a large void [26]. Note here that measures of void volume, e.g., porosity, whether local or global, cannot comprehensively distinguish heterogeneous from homogeneous patterns in connectivity. By contrast, with the exception of degree, basic network measures such as clustering coefficient, subgraph centrality and network bipartivity, can detect details in the arrangements of contacts down to the fine scale of a particle and its neighbours. This is important for understanding how and why *emergent* functional mesoscopic structures form during the material's loading history.

While detailed studies with a special focus on force chains and their laterally supporting cycles bear obvious significance, a broader system-wide examination of the connections in the material is equally important. Thus, we will complement the study of the aforementioned feature vectors with an investigation into the nature of k-cores and their complement graphs. In social and biological networks, k-cores have proven to be particularly effective in understanding the evolution of well-connected versus least-connected parts of a given network (see, for example, [34] and references therein). Here we will explore the sequence of collapse or fragmentation of the maximum k-core and the extent to which it can provide useful insights into the loss of stability, and the importance of high connectivity and clustering in the formation and preservation of load-bearing force chains.

The article is arranged as follows. Details of the simulations are provided in Section 2. As stated earlier, the three samples considered here provide an opportunity to explore how material properties and boundary conditions influence the evolution of connections in the various networks as the material deforms. The complex networks analysis in Sections 3–4 then aims to demonstrate the losses and gains in functional connections, particularly of the force chain network, and how this is influenced by important factors long known from experiments to govern bulk behaviour, i.e., particle shape, modelled by a rolling resistance at contacts, and confining pressure [14]. Concluding remarks are given in Section 5.

2. Simulation details

The three samples studied here from a complex networks perspective are part of an extensive suite of DEM simulations discussed in great detail and length in [35] and [36]. Precise mathematical details of the contact laws and material properties can be found in [35]. The three chosen samples differ from each other by boundary conditions – constant confining pressure verses constant volume – and value of the rolling friction coefficient. The size of each sample is 5098 particles which is of the same order as a physical photoelastic disk experiment comprising 1000 particles which we are currently examining: [31,32] and [27]. It is also consistent with numerous simulations reported in the geomechanics literature: [37–40] are but a few examples. Furthermore the values of friction coefficient were chosen to establish persistent and relatively clear shear band boundaries.

In broad terms the DEM model considered in [35] and [36] consists of a two-dimensional polydisperse assembly of circular particles subject to biaxial compression throughout the deformation history. Resistance to relative motion at the particle–particle and particle–wall contacts is governed by combinations of two linear springs, two dashpots and a friction slider. The model is designed to mimic the response of assemblies of noncircular particles. Thus, it incorporates a moment transfer to account for rolling resistance, in accordance with [2,41]. This modification to the classical DEM model of [11], which allows the relative rotations of particles at contacts to be controlled, has been found to be essential in achieving more realistic rotations and stress predictions (e.g., [8]).

The vertical walls are frictionless, so that particles can slide and roll along them without any resistance; otherwise, all other material properties are identical to those of the particles. The top and bottom walls are assumed to have the same material properties as the particles. The stiffness coefficient for the rolling resistance is chosen based on the assumption that, under equilibrium conditions, contact moments due to rolling resistance are comparable to the moments due to the tangential forces [35].

Of interest here is the response of the three assemblies upon commencement of biaxial compression under a constant strain rate in the vertical direction of $\dot{\varepsilon}_{yy} = -0.008\ \mathrm{s}^{-1}$. (Both $\dot{\varepsilon}_{yy}$ and σ_{yy} have been taken as negative in compression.) Additional simulations performed at even smaller rates of deformation confirmed that the strain rate is sufficiently small and σ_{yy}/k^n, k^n the normal spring stiffness, is sufficiently low to ensure quasistatic conditions and a persistant shear band, respectively, see [35].

Two of the samples, referred to hereafter as "CP1" and "CP2", are allowed to expand in the horizontal direction under identical constant confining pressures; the third sample, referred to as "CV", is compressed under constant volume and

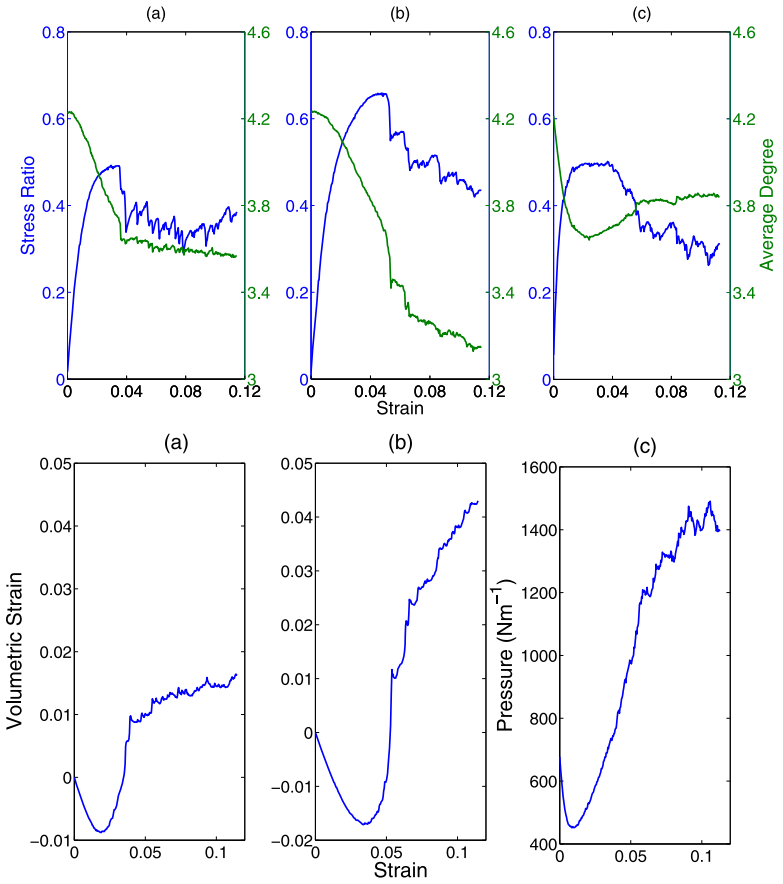

Fig. 1. Top: strain evolution of stress ratio and number of contacts per particle (degree) for samples (a) CP1; (b) CP2; (c) CV. Bottom: strain evolution of the volumetric strain for samples (a) CP1; (b) CP2; and the pressure for (c) CV.

varying confining pressures. Moreover, upon commencement of biaxial loading, the two samples, CP1 and CP2, are given distinct contact rolling resistance parameters: the rolling friction coefficient is $\mu_r = 0.02$ for CP1 and $\mu_r = 0.20$ for CP2. The third sample CV is identical in material properties to sample CP1. The strain evolution of the system exhibits distinct regimes of deformation, typically seen for dense cohesionless granular assemblies (e.g., dry sand under plane strain biaxial compression): a period of strain-hardening, followed by strain-softening and, finally, the so-called critical state regime (see Fig. 1. N.B. the average degree is also shown on the stress ratio plot to facilitate the discussion in Section 3). The strain-hardening regime is characterized by a monotonic increase with axial strain of the shear stress to a peak value, with the applied shear stress being given by the stress ratio $(\sigma_{yy} - \sigma_{xx})/(\sigma_{xx} + \sigma_{yy})$. Post peak, relatively large fluctuations are evident: the ensuing strain-softening regime is characterized by a sequence of precipitous drops in the shear stress ratio before reaching the critical state regime at which point the shear stress ratio fluctuates about: an essentially steady-state value in CP1, and a decreasing value albeit at a considerably slower rate than before in CP2 and CV.

In all the three samples, the onset of the so-called persistent shear band initiates just before the peak shear stress. The post-peak regime encompasses the continuation of the development of the shear band and the ensuing near steady-state evolution of the band. The shear band is fully formed at the following axial strains for the three samples: $|\varepsilon_{yy}| = 0.04$ for CP1, $|\varepsilon_{yy}| = 0.0534$ for CP2; $|\varepsilon_{yy}| = 0.0562$ for CV. Consecutive cycles of unjamming–jamming events (i.e., drop and rise in macroscopic shear stress) are evident and are reminiscent of the so-called "slip-stick" phenomenon observed in other granular systems [42–44]. These have been attributed to the continual collapse of old and regeneration of new force chains inside the shear band and reflect the low level of packing within the sample. The stick-slip phenomenon disappears as the continuum limit is approached for larger packings. Deformation is highly heterogeneous and relatively high porosity regions develop inside shear bands in all three samples.

We found from previous studies that the dilatation in the shear band is governed by the buckling of force chains; buckling is not only an inherently dilatant mechanism but one that also induces dilatant rearrangements in the surrounding particles [35,45,31].

3. Granular networks

A network or graph is a collection of nodes and links. At any given strain state, a (complex) contact network can be constructed in which the particles are cast as the nodes of the network and a connecting link or edge exists between two particles that are in contact. Particle rearrangements in the quasistatically deforming granular material will be reflected in the evolving network: some old network connections break as contacts are lost, while some new connections form as contacts are created. The contact network is an unweighted, undirected graph and is usefully summarized by an adjacency matrix. Complex networks offer a multitude of statistical measures for the quantitative characterization of evolving networks, many of which can be calculated by manipulating the adjacency matrix. In two-dimensions a granular contact network is a planar graph but we deliberately refrain from exploiting this property as ultimately we want useful complex network measures for three-dimensional granular systems.

While the contact network focusses solely on connectivity in the deforming granular material, other aspects of the material may be incorporated into the analysis by appeal to weighted graphs. For instance, we may weight each connecting link with the magnitude of the contact force and then similarly probe the statistics of this evolving weighted network. In a similar vein, we may also focus on specific subgraphs of both the unweighted and weighted contact networks to uncover particular aspects of the material (e.g., regions of high connectivity in k-cores, cyclic motifs in minimal cycles, to name just a few examples). We now discuss these in detail below.

3.1. Feature vectors

Sample CP1 was the primary system studied using network techniques in [19]. In the present work we extend the study of degree, clustering coefficient, subgraph centrality, network bipartivity to the new samples CP2 and CV to compare and contrast the effect of rolling resistance and boundary conditions. Furthermore, we discuss other network structures such as n-cycles and k-core subgraphs to reveal further insights into the fabric of each sample.

The granular assembly responds to increasing compression through rearrangements of its particles. This rearrangement is reflected in an evolving contact network which can be summarized succinctly by a feature vector. Feature vector is a name given to n-tuples of network measurements [25]. Feature vectors therefore are points in an n-dimensional (feature) space. The trajectory of feature vectors in feature space gives valuable insights into the response of the material. In the following, we describe four measurements of a complex network which can be used to construct feature vectors: degree, clustering coefficient, subgraph centrality and network bipartivity [22,23,25]. The evolution of these n-tuples as the material responds to biaxial loading elucidates functional activity in the lead up to and during the critical state regime.

One of the most fundamental properties of a network is its degree distribution. The degree of a node i is simply its total number of links:

$$k(i) = \sum_j a_{ij} \tag{1}$$

where a_{ij} is an entry of the adjacency matrix ($a_{ij} = 1$ for a contact and is equal to zero otherwise). This can be averaged over all particles in the assembly (including rattlers) and is closely related to the so-called coordination number of a particle which represents its total number of contacts. Interest in classifying networks by their degree distribution has driven research on complex networks with special attention being given to a system exhibiting either small-world properties or a scale-free degree distribution [20,21]. In our case the degree distribution is neither scale-free nor exhibits small-world properties. This is clear since the particle size distribution of all our samples only allows a particle to have maximum degree equal to 7 and since the contact network is in essence a geographical network – direct physical contact defines a link – there can be no network hubs characteristic of scale-free networks. Likewise, shortcuts or long-range links connecting distant particles which typify small-world network structures are not possible for our samples.

Recall Fig. 1 shows the strain evolution of average degree for contact networks of the three samples. In the initial period of loading, prior to peak shear stress, the average number of contacts per particle in all three samples decreases monotonically with axial strain. This common trend reflects the degeneration of contacts in the direction of extension. Loss of connectivity, measured by the rate of decrease in degree, is greatest for CV where the varying confining pressure over this period of loading is always less than that applied to the dilating samples CP1 and CP2. For strains around the peak shear stress, the average degree reaches a minimum. In sample CP1, the average degree reaches a minimum just after peak and then subsequently saturates (modulo fluctuations) as the rate at which contacts are lost is balanced by the rate at which new contacts are formed; for sample CP2, we observe a continuing but markedly milder decline than before peak. Immediately after peak shear stress, we observe a precipitous drop in degree for the dilating samples CP1 and CP2. The drop in degree is much greater for CP2: it undergoes, on average, a much greater loss of contacts per particle at peak failure. Despite this, the higher rolling resistance operating at contacts in CP2 contributes to the system being able to sustain a higher load (higher peak shear stress) and a more delayed failure point than CP1.

There are quantitative differences in the strain evolution of the shear stress of the CV sample compared to that for CP1 due to the higher confining pressure acting on CV: as can be seen in Fig. 1, there is slightly longer and flatter evolution of the shear stress towards peak for CV. The confining pressure for CV, which commences at a value equal to that applied

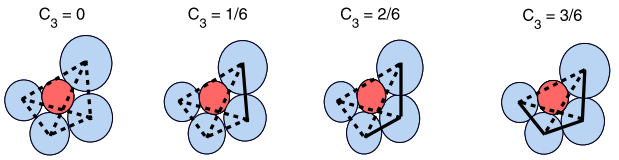

Fig. 2. Mesoscopic arrangements present in the samples of five particles and the clustering coefficient of the central particle with degree equal to four. The six theoretically possible contacts between the central particles neighbours in the abstract complex network are shown as dotted lines, actual contacts are represented by the solid lines.

to CP1 and CP2, decreases initially to a minimum of 451.62 $\mathrm{N\,m^{-1}}$ at $|\varepsilon_{yy}| = 0.0088$, then rises steadily to a maximum of 1490.1 $\mathrm{N\,m^{-1}}$ at $|\varepsilon_{yy}| = 0.1059$ before levelling off; the confining pressure for sample CV is greater than that for samples CP1 and CP2 for strains beyond $|\varepsilon_{yy}| = 0.0324$. Consistent with this evolution in confining pressure, the average coordination number for sample CV reaches a minimum just before peak stress, then rises for a brief period, before essentially leveling off. We note here that throughout the loading history, rattlers are present, which were included in the calculation of average coordination number. Rattlers are particles with at most one contact and are free to move within a cage formed by their first ring of neighbours as defined by a Delaunay triangulation [45]. In what follows, we will probe the underpinning micromechanics behind the increase in degree prior to critical state in CV using feature vectors and other physical measures.

Consideration of n-tuples as feature vectors, in addition to studies of strain evolution of individual network properties can significantly enhance the information we can extract from complex networks. To proceed, we need to compute other network measures besides degree. Of particular interest here are measures that, unlike degree, can distinguish heterogeneities in the local arrangements of particles, i.e., contact anisotropy in local particle neighbourhoods. For this we turn our attention to the next fundamental property of a network: the clustering coefficient [20]. The clustering coefficient is concerned with the connectivity of a particle and its contacting neighbours, i.e., the mesoscopic scale. As it locally quantifies the number of triangles, or 3-cycles, associated to a particle it gives more information about fabric anisotropy than degree alone. When the clustering coefficient for each particle (excluding rattlers) is averaged over the whole assembly it provides one measure of the number and density of 3-cycles in a network. In a 2D granular assembly of particles the 3-cycles in its contact network have a very important interpretation, i.e., frustrated rotations. Three particles in mutual contact and thus arranged as a triangle, frustrate each others propensity to rotate and so enhances the stability of structures containing these 3-cycle member particles. The clustering coefficient can be easily calculated for each particle and its evolving distribution studied. For each particle we find its contacting neighbours and count how many of those neighbours are in contact with each other. The ratio of this number to the number of possible contacts between each of the particle's neighbours (given by $k_i(k_i - 1)/2$, where k_i denotes the number of neighbouring particles) is the clustering coefficient of that particle. Mathematically [29]:

$$c(i) = \frac{1}{k_i(k_i - 1)} \sum_{j,h \in V(i)} a_{ij} a_{jh} a_{hi} \tag{2}$$

where k_i is the particle degree defined above and $V(i)$ is the set of contacting particles of i. For example, consider the mesoscopic arrangements of five particles as shown in Fig. 2 where the clustering coefficient of the central particle is given. We note, that these are actual particle configurations found within our samples. Here, the degree of the central particle remains fixed but as the surrounding particles rearrange (possibly through the mechanism of relative rotations) triangles are formed and the (local) clustering coefficient changes thus reflecting the local fabric anisotropy. The incremental changes to clustering coefficient clearly depend on the degree of the central particle and we also note that a clustering coefficient of unity is not possible for degree greater than 2 due to the physical constraints of the system. That is, not all connections between a central particles' neighbours are possible although they are counted in the denominator of the clustering coefficient.

Considering the feature vector 2-tuple consisting of the averages of degree and clustering coefficient together and following its evolution in feature space, the transition through the strain-hardening regime and the collapse to the critical state is evident. In Fig. 3, we show these in the form of scatter plots of pair-wise projections of the feature vectors for the three samples. Initially (top right of trajectories in Fig. 3), both the degree and clustering coefficient are high. As strain increases and the material undergoes strain-hardening to peak shear stress, the average degree monotonically decreases, as does the clustering coefficient in all of the samples. At failure or at the onset of the critical state, these features appear to have collapsed to an equilibrium point, in which a near constant degree and clustering coefficient is attained. This is to be expected since the distributions shown earlier in Fig. 1 show a near steady state behaviour in the critical state regime, especially for CP1.

For CP2, the stationary point representing the critical state is at a very low average degree and clustering coefficient. Hence, from the clustering coefficient, we see that there are fewer stabilizing triangle configurations in the CP2 sample as compared to the CP1 sample in critical state; here again we observe that the higher rolling resistance helps to defend against the destabilizing effects of loss of connectivity. In other words, the CP2 sample, by virtue of the higher rolling resistance operating at all of its contacts, can adopt a much sparser yet stronger contact network with a higher peak load-carrying capacity, delayed failure point (i.e., strain at which peak stress is reached), and residual strength (load-carrying capacity in the critical state).

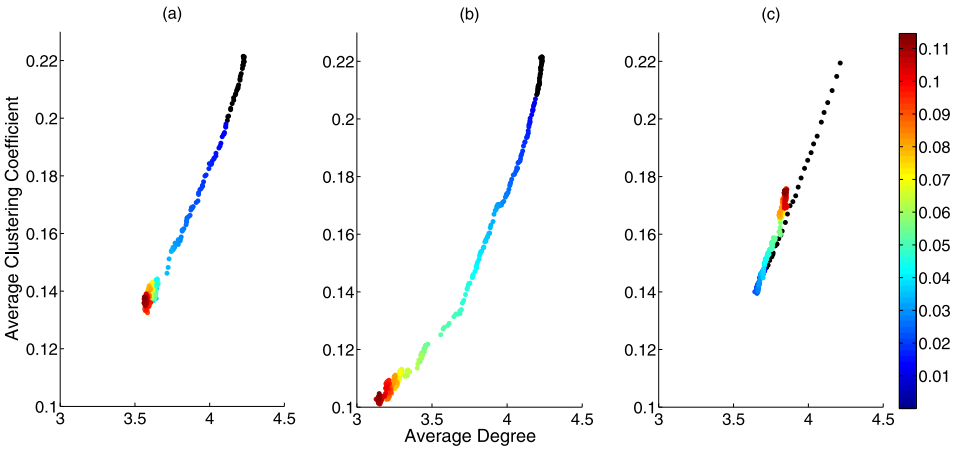

Fig. 3. Feature space projections for the unweighted contact network for samples (a) CP1; (b) CP2; (c) CV: clustering coefficient versus degree. Changing colour from blue to red indicates strain evolution from start of loading through to critical state. (For interpretation of the references to colour in this figure legend, the reader is referred to the web version of this article.)

For CV, the sample compressed under constant volume, we observe a "loop back": the trajectory reaches a minimum of degree and of clustering coefficient, then reverses in trend with both degree and clustering coefficient increasing until the critical state is reached.

The clustering coefficient described above concerns triangle motifs in the network, the lowest order in the minimal cycle basis. Another prevalent network motif in a contact network is the 4-cycles, or "squares". A clustering coefficient for squares can be calculated in a manner similar to that described above for 3-cycles (see, for example [24], where a 4-cycle coefficient is introduced analogous to the 3-cycle clustering coefficient above). It is reasonable to ask if there is a network measure which reflects the aggregate of all of the n-cycles present in a network. Indeed there is: namely, subgraph centrality and its close relative, network bipartivity, introduced by Estrada and Rodríguez–Velázquez in [22] and [23]. The subgraph centrality of a particle is a weighted sum of the number of closed paths in the network originating and terminating at that particle. Specifically,

$$C_s(i) = \sum_{k=0}^{\infty} \frac{\mu_k(i)}{k!} \tag{3}$$

where k is the cycle length, and $\mu_k(i)$ is the number of paths of length k for particle i. A more computationally tractable formula for subgraph centrality can be found in [22]. The sum is weighted by a factor depending on the length of the path because the count does not exclude non-self-avoiding paths – paths which retrace steps to construct closed paths – and so the count for each particle would be infinite without this normalizing factor. A consequence of the weighting is that low-order cycles receive more weight in the sum. As was the case with degree and clustering coefficient we can average over all particles in the assembly to obtain an average value of subgraph centrality $\langle SC \rangle$.

The network bipartivity is closely related to subgraph centrality; in fact, it is a measure of the contribution to subgraph centrality solely by even length closed paths. The network bipartivity lies between $\frac{1}{2}$ and 1 and the closer it is to one reflects the paucity of odd-cycles in the network. If the network bipartivity is equal to 1 then the network is bipartite, i.e., there exists no odd-cycles in the network. The network bipartivity of a complex graph G, is given by:

$$\beta(G) = \frac{\langle SC \rangle_{even}}{\langle SC \rangle} \tag{4}$$

where $\langle SC \rangle_{even}$ is the subgraph centrality of even closed walks. A more computationally tractable formula for network bipartivity can be found in [23].

The feature space evolution of the subgraph centrality with degree is qualitatively the same as the evolution of the clustering coefficient and so is not shown. It captures the collapse post peak shear stress and an evolution to a stationary distribution in the critical state. The "loop-back" for the CV sample is also evident. Furthermore, the fall in subgraph centrality for CP1 and CP2 suggests that not only are the presence of odd 3-cycle configurations decreasing, 4-cycle configurations are also being destroyed by the continual loading. Moreover, the lower relative value of subgraph centrality in the CP2 sample as compared to CP1 demonstrates the effect a higher coefficient of rolling friction has on stability. Relatively fewer low order cycles are present in CP2 and yet it can sustain higher loads before failure than CP1 which has more low order, and hence more stable, cycle configurations.

The feature space plot of network bipartivity can help reveal if the loop-back of subgraph centrality is due to an increase of low order even cycles or an increase of low order odd-cycles. In Fig. 4, for CV we observe a fall in network bipartivity

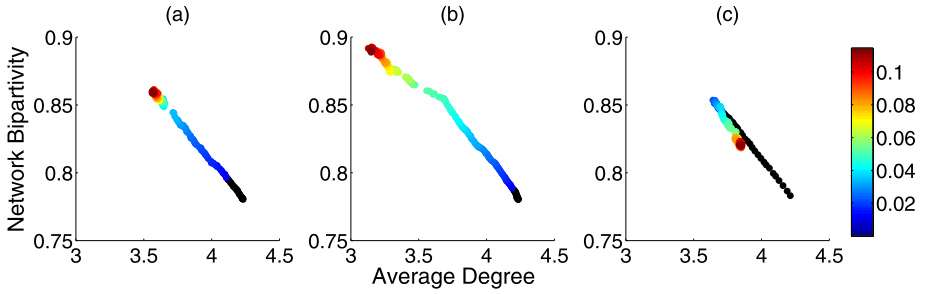

Fig. 4. Feature space projections for the contact network for samples (a) CP1; (b) CP2; (c) CV: average network bipartivity versus average degree. Changing colour from blue to red indicates strain evolution from start of loading through to critical state. (For interpretation of the references to colour in this figure legend, the reader is referred to the web version of this article.)

which translates to a relative increase in the prevalence of odd-cycle configurations, and as seen from the clustering coefficient, this is mainly 3-cycle configurations. That is, the effect of an increase in confining pressure in the CV sample is to evolve its connectivity towards a less bipartite network – that which attains more stabilizing odd-cycles. The question then is how uniform is the distribution of these low order cycles in the CV sample as compared to the constant pressure samples? To shed light on this question, we probe more closely the commonalities and differences in the trends seen for the dilatant versus constant volume samples. It is reasonable to expect that the progressive dilatation that first occurs throughout the sample in the initial stages of the strain hardening regime is what is responsible for the initial decrease of clustering coefficient (Fig. 3) as well as subgraph centrality. Indeed the spatial distributions of the network properties show this is the case for all the three samples.

3.2. k-cores

The loss of connectivity can be further investigated by examining the k-core of a network [34]. It is defined as the largest subgraph in a network whose vertices have degree at least k. We generate the k-cores, subgraphs of the global contact network, by recursive pruning of the vertices from the graph whose degree is less than k. The links of a network can be decomposed into three groups: those links which connect nodes within the k-core (the k-core network), those links which connect nodes not belonging to the k-core (the k-core complement network), and links which span nodes in the k-core and its complement. Where the k-core exists the material has the strongest connectivity. The absence of the k-core in any area is indicative of the poor stability of that region.

The k-cores of a contact network are informative. The 1-core removes all of the degree zero rattlers – particles that for a particular axial strain value are completed isolated. The 2-core removes the rattlers and all "straggly" bits of the network leaving only those particles which make up the minimal cycle basis of the network. Minimal cycle bases reveal a great deal about the structure of a complex network. The changing distribution of n-cycles moulding the contact network shows the manifestation of the effects of decreasing stability – reduction in 3-cycles as quantified by the clustering coefficient – and dilatation – an increase in the population of higher-order cycles. We found the maximum value of k where a k-core exists in all three samples is $k = 3$ and the changing structure of the 3-core is startling as the loss of connectivity within the material is disclosed. It is worth pausing to inspect the features of the 3-core network which is shown in Fig. 5.

The number of connected components in the 3-core, and indeed any network, can be obtained through a spectral analysis of the Laplacian matrix although more efficient algorithms exist. We used an algorithm due to [46] to find the number of connected components as is shown in Fig. 6. Here, we calculate how many connected components the 3-core fractures into for each sample. We see that, typically, the number of components in the 3-core is one, i.e., the 3-core is a single-connected graph – until the onset of shear banding, at which point the 3-core fragments into multiple connected graphs. In particular, throughout loading the 3-core network of CP1 loses connectivity until it splits around the peak shear stress. Thereafter, its number of constituent parts remains relatively invariant, in the sense that there are essentially two main components for the rest of loading: these components are shown for a particular strain value in Fig. 5(a). The algorithm of [46] can also be used to quantify the relative sizes of the component 3-cores. Note that the data given by the solid line in Fig. 6 do not give an indication of the relative sizes of the component 3-cores. By filtering out small components, e.g., less than 10% of the initial 3-core at start of loading, we find the main components of the 3-core that essentially represents the regions outside of the shear band (Fig. 6 (red) dashed line). We find here that the fluctuations in the number of components of CP1 in Fig. 6(a) is due to small islands or component 3-cores forming intermittently within the sample (see, for example, Fig. 5(a) and (b)). These islands usually reside adjacent to edges of the shear band and represent small clusters comprising only a few particles. Overall, these results suggest that the separation of the 3-core network coincides in time (strain) and space with the development of the shear band.

For the CP2 sample, the fragmentation of the 3-core around the peak shear stress is far more severe than CP1. Comparing Figs. 6(a) versus 6(b), we observe a considerably higher number of components after the initial split of the 3-core in CP2. It is interesting to juxtapose these patterns of fragmentation against the earlier trends discussed in the preceding section

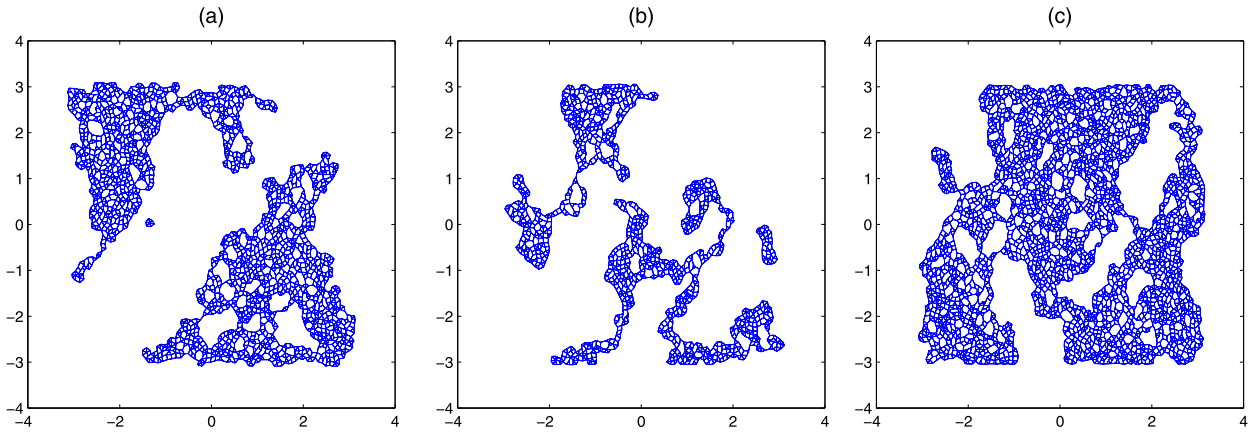

Fig. 5. Maximum core, i.e. 3-core, captures regions of high connectivity in the material. This initially singe-connected graph splits into multiple components in the critical state regime: (a) $|\varepsilon_{yy}| = 0.04$ for CP1; (b) $|\varepsilon_{yy}| = 0.0534$ for CP2; (c) $|\varepsilon_{yy}| = 0.0562$ for CV. Note the fragmentation pattern often results in the intermittent presence of small components during failure.

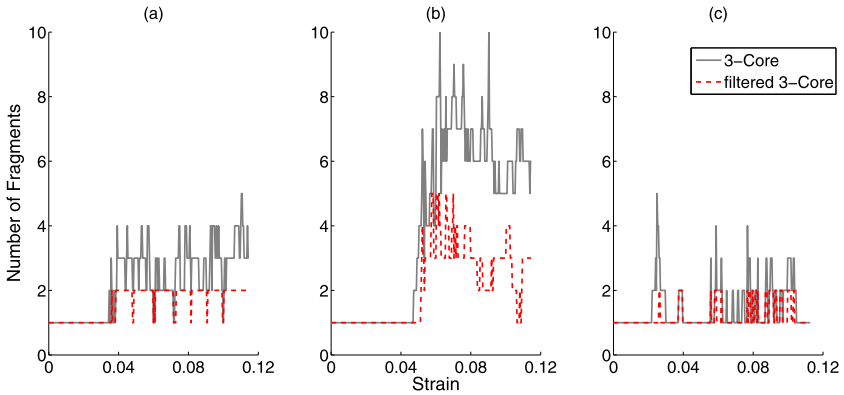

Fig. 6. Fragmentation of 3-core reflects breakdown of functional connectivity at key stages in the loading history. Strain evolution of the number of fragments or singly-connected graphs in each k-core (a) CP1; (b) CP2; (c) CV. The 3-core definitively splits when persistent shear band for each sample is fully evolved. Small islands have been filtered out to reveal largest 3-cores that essentially represent the main regions outside of the band.

Table 1
Strain $|\varepsilon_{yy}|$ values of trigger force chain buckling event, fully developed shear band and strain interval between both for all three samples.

Sample	Trigger (strain)	Fully developed (strain)	Period from trigger to total failure
CP1	0.03	0.04	0.01
CP2	0.0477	0.0534	0.0057
CV	0.0308	0.0562	0.0262

on feature vectors for these two samples. Despite the widespread decimation of the connectivity in CP2 in the lead up to and during the critical state regime, the higher rolling resistance enables the material to: carry a much higher peak load, survive longer before failure as evident in the strain state at which sudden drop from peak stress occurs, and bear a higher residual load in the critical state.

In the CV test, the 3-core also separates into two main components but periodically coalesces into one large and single-connected graph. This is because the shear band forms a V-shape in which each side of the "V" develops and persists in alternating intervals of strain, leading to a somewhat intermittent evolution rather than a steady fragmentation of the sample into three component 3-cores.

Common to all three samples is the unequivocal spatial correlation (Fig. 7) between the location of buckled force chains and their confining particles (CFBCs) and absence of 3-core: force chains buckle in areas where the 3-core does not exist (the 3-core complement). Differences in the samples occur after the buckling initiates. It does not take many more strain states from trigger buckling (i.e., initial buckling) for CP2 to reach total failure (Table 1). The period from trigger buckling to total failure is longest for CV – the effect of the lateral support given by increasing confining pressure – and smallest for CP2. For CP2, while the loading is increased, the rolling resistance provides strength to force chains but at the same time the network becomes progressively sparse (recall the lower average degree and average clustering coefficient from the feature

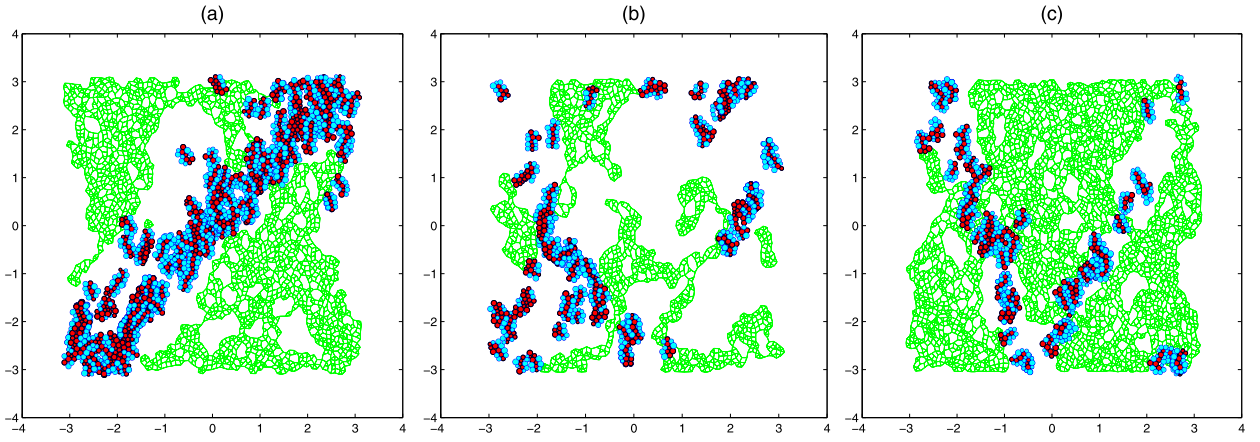

Fig. 7. The maximum core, 3-core, in the shear banding regime together with CBFCs: (a) $|\varepsilon_{yy}| = 0.04$ for CP1; (b) $|\varepsilon_{yy}| = 0.0534$ for CP2; (c) $|\varepsilon_{yy}| = 0.0562$ for CV. A cumulative plot of buckled force chains (red) is shown along with their confining neighbours (blue) starting from the strain state of the trigger force chain buckling event to full formation of the band for each sample. (For interpretation of the references to colour in this figure legend, the reader is referred to the web version of this article.)

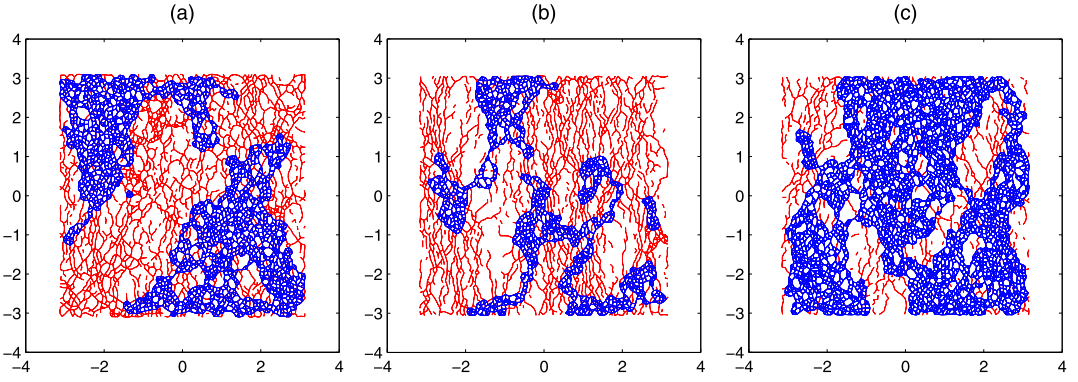

Fig. 8. Snapshot of the 3-core (blue) plus strong links (red) network which encompasses 99% of force chains particles and links: (a) $|\varepsilon_{yy}| = 0.04$ for CP1; (b) $|\varepsilon_{yy}| = 0.0534$ for CP2; (c) $|\varepsilon_{yy}| = 0.0562$ for CV. (For interpretation of the references to colour in this figure legend, the reader is referred to the web version of this article.)

vector analysis). These force chains are very strong by themselves, but they do not have strong, or sufficient, lateral support. Thus, once a force chain buckles, the domino effect will take place and buckling will cascade to all the other force chains. Examining the spatial distribution of CBFCs, we can see the force chains that buckle are located in the region outside the 3-core (i.e., the region with less connectivity).

4. Functional activity

In the previous sections, we have introduced new techniques for micromechanical studies of granular materials that focus on the evolution of connectivity in biaxial compression tests. These techniques encompass complex network concepts of minimal cycles, feature vectors of various measures of connectivity including 3-cycle memberships (clustering), and k-cores. We will now connect these techniques and the insights derived from them to the building blocks of granular materials, i.e., force chains and 3-cycles. In particular, our aim here is to demonstrate the co-evolution in these structures to reveal underpinning dynamics and functional activity. These structures and their cooperative evolution are common to all of our samples and we believe are generic to dense granular assemblies under loading. To uncover underpinning dynamics and breakdown of functional connectivity, the strategy we adopt is to overlay information from complex networks with existing knowledge on force chains and their evolution.

To begin with, we consider the intersection set of two subnetworks: (i) the 3-core which is that part of the contact network with the highest connectivity, and (ii) the strong links which are the contacts carrying above-the-global-average force. This intersection set yields a network that captures above 99% of the force chains throughout loading (Fig. 8). Thus the force chain network must necessarily span both the 3-core and its complement to allow the sample to continue to resist the applied load. Results that show the strain evolution of the percentage of force chain particles in the 3-core and of the percentage of buckled force chain particles in the 3-core complement support this finding. Fig. 8 is indicative of the process by which force chains fail: here we see that force chains which span the 3-core complement are connections which carry

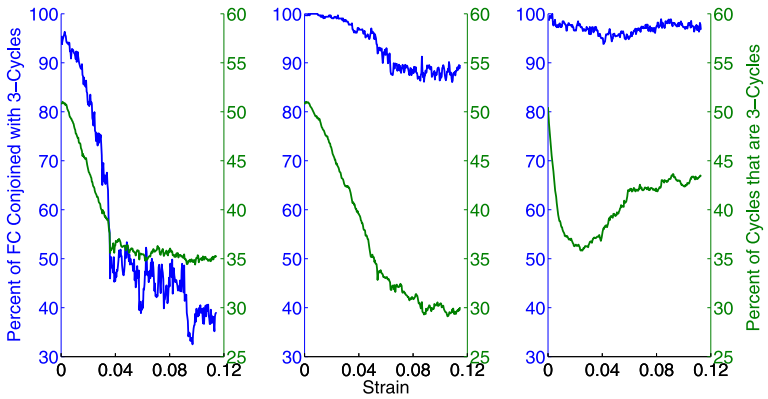

Fig. 9. Strain evolution of percentage of force chains conjoined with 3-cycles and population of 3-cycles expressed as a percentage relative to all cycles.

the majority (above-the-global average) of loads – *under minimal or no lateral support*. It thus comes as no surprise that these chains then become prone to buckling – and indeed fail by buckling – whereas their counterparts in the 3-core remain essentially unscathed by this failure process. Compelling evidence of this resides in the CBFCs – nearly all of which are in the 3-core complement (the few that are not are generally next to walls). This property appears to be generic to all three samples.

We next look to possible co-evolution between 3-cycles and force chains. We know from previous studies that the 3-cycle population signified by the clustering coefficient plays an important role in frustrating relative rotations between constituent particles [26]. Thus these 3-cycles when conjoined with particles from load bearing force chains effectively act as trusses. As demonstrated in Fig. 9, most force chains are conjoined with 3-cycles, suggestive of the support that these granular trusses provide. Specifically, force chains receive dual support from 3-cycle trusses: (i) they reduce the relative rotation between and with force chain particles thereby impeding buckling, and (ii) they provide lateral support by "propping-up" the force chain. The benefits of this dual support are available and, as expected, manifest themselves to varying degrees in all three samples. By virtue of the increased rolling friction coefficient in CP2, 3-cycles can suppress rotations to a greater extent than those in CP1 and as such fewer 3-cycles are required to achieve this. On the other hand, the extent to which the 3-cycles can prop-up or provide strong lateral support to force chains depends on the confining pressure and hence this effect is more pronounced in CV compared to the dilatant samples. Compared to CP1, the population of 3-cycles is higher in the CV sample in the critical state and the fact that more support is given to the force chains in CV in this regime manifest in the longer strain interval from the onset of the shear band, as marked by the trigger (initial) buckling, to the full development of the shear band (Table 1). In effect, the increase in confining pressure of the CV sample to preserve constant volume means that although the trigger failure of force chains occurs at the same state as the same material but under constant confining pressure CP1, the greater lateral support to force chains in CV staunches the spread of failure throughout the sample. This results in a longer strain interval for the shear band to fully develop and even when it is fully formed, in the shape of a "V", each wing is temporally and intermittently reinforced.

Tordesillas et al. [26] introduced the concept of 3-force cycles – 3-cycles whose contacts each carry above-the-global average force. These force cycles have a close relationship to force chain buckling. As with 3-cycles, most of the 3-force cycles are conjoined with force chains, even though only a small percentage of force chains have 3-force cycles for support: see Fig. 10. In general, 3-force cycles tend to concentrate inside shear bands and in the regions where different parts of the shear bands intersect (in cases where the band has multiple parts as in samples CP2 and CV). Common to all three samples, new 3-force cycles emerge in areas where the material requires these extra reinforcements, namely, from the onset of buckling and in the shear band region where buckling is confined and where resident force chains bear nominal lateral support.

While the 3-force cycles may prolong the life of buckling force chains during shear banding, their effect on force chain lifetimes is intermittent at best. We explore this by considering the onset of shear banding in all samples as signaled by the buckling of force chains. Recall the first buckling event is referred to as the trigger event. Lifetimes of 3-force chains born at a given strain state are examined. Here a force chain is said to be born at a given strain state if it is identified as a force chain at that state but was not classified as a force chain in the preceding strain state. The lifetime is then the strain interval from birth to the last recorded strain state during which it is classified as a force chain. A key question that arises here is: do force chains born before the trigger buckling event exhibit different lifetime patterns to those born after this event? The mean lifetimes do not appear to be significantly affected by the presence of buckling or during that regime where new 3-force cycles are seen to increase within the samples. However, there is a statistically significant difference (KS-test) in the frequency distributions of lifetimes for strain states prior to versus after trigger event in the dilatant samples but not the constant volume sample. A possible explanation for this is the effect stronger lateral support to force chains acting on the CV sample has on the length of the strain interval between trigger buckling and full development of the shear band. Since increasing pressure helps prolong force chain lifetimes drawing a strict boundary to compare force chain lifetimes before

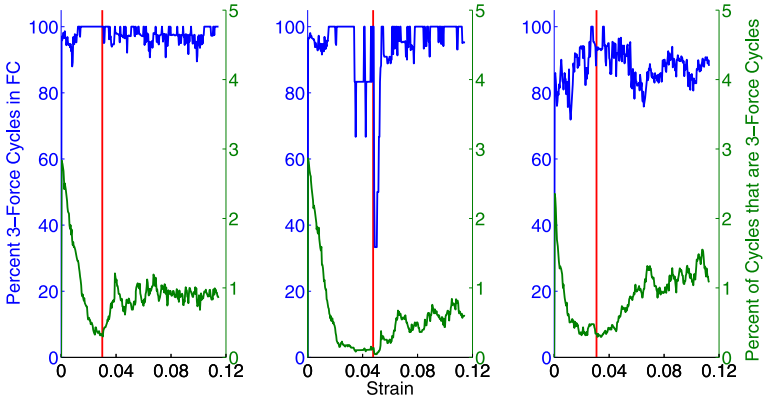

Fig. 10. Strain evolution of percentage of 3-force cycles in force chains and population of 3-force cycles expressed as a percentage relative to all cycles. The trigger buckling event indicated by the (red in the web version) vertical line.

and after is less definitive compared to the shorter strain intervals for shear band development in the constant pressure samples.

5. Conclusion

Studies of network connectivity and their evolution in three distinct samples under biaxial compression – two of which are under the same constant confining pressure while a third is under constant volume – reveal generic functional activity. Patterns of evolution in the contact networks, quantified through feature vectors, k-cores, and minimal cycles, suggest an intrinsic structural hierarchy which utilizes force chains as primary load-bearing columns, laterally supported by 3-cycles that act as trusses. By overlaying information on force chains and force chain buckling with network features, we uncover important dynamics and patterns of evolution in functional connectivity. The breakdown of 3-cycles, as revealed in the feature vectors, along with the increasing load borne by the force chains as loading proceeds, leads to loss of stability and ultimately failure of force chains by buckling. In particular, we found that the great majority of force chains are supported by 3-cycles. Force chains which buckle are those which span the 3-core complement, the region of lowest connectivity. In this region where reinforcing 3-cycles are in short supply, force chains appeal to 3-force cycles. These are the strongest 3-cycles which consequently offer dual resistance to buckling: frustrated rotation and strong lateral support.

Differences in the evolution of functional connectivity between the samples can be tied to the difference in material properties and boundary conditions. Higher rolling resistance allows force chains with minimal lateral support (fewer 3-cycles) to survive longer. But once failure initiates, the spread of failure is more extensive throughout the sample, akin to a “domino effect”. The presence or absence of the 3-core and the fragmentation pattern of the 3-core are indicative of the spatial extent of failure. The increase in confining pressure of the CV sample to preserve constant volume also has ramifications on the failure propagation. Although force chain buckling initiates at the same state as CP1, the same material but under constant confining pressure, the greater lateral support to force chains in CV obstructs the spread of failure throughout the sample. This results in a longer strain interval for the shear band to fully develop and, even when it is fully formed into the shape of a “V”, in which each wing is temporally and intermittently reinforced.

3-cores capture the spatial and temporal (strain) evolution of failure from the onset of shear banding. The force chain network when overlaid with the 3-core complement reveals the scant lateral support to force chains in these regions of low connectivity – which helps to explain why these force chains buckle and those in the 3-core do not. The finding that nearly all buckling events occur in the 3-core complement supports this. Once the process of buckling initiates, force chain buckling perpetuates further loss of connectivity. Buckling voraciously eats away at the material’s connectivity, with significant loss of connectivity invariably observed in the locality of and immediately following buckling events – ultimately leading to the fully developed shear band. The fragmentation of the 3-core corroborates past knowledge on force chain buckling events, and particularly the strong correlation between force chain buckling and the mechanisms of nonaffine deformation and dilatation.

Rheological models of granular materials crucially depend on a thorough understanding of the evolution of contacts (fabric) and contact forces to deliver reliable and robust predictions. The use of complex network statistics and subnetwork structure has helped uncover new insights into and quantify the differences and similarities in these aspects of material behaviour more comprehensively than past micromechanical studies of granular samples in similar soil mechanics tests. We thus envisage complex networks to be a promising new toolbox for soil micromechanics, with even greater potential if fused with other areas of mathematics and mechanics, e.g., dynamical systems, optimization and structural mechanics. Future research will examine these synergetic blends of approaches, as well as continue to introduce new measures from complex networks, especially in three-dimensional systems with detailed attention given to the propagation of failure.

Acknowledgements

This work was supported by US Army Research Office (W911NF-07-1-0370) and the Australian Research Council (DP0986876 and DP0772409). We also thank the Victorian Partnership for Advanced Computing for computing resources. We thank the anonymous reviewer for suggesting changes which have significantly improved the manuscript.

References

[1] J.P. Bardet, J. Proubet, The structure of shear bands in idealized granular materials, Applied Mechanics Reviews, ASME 45 (1992) S118–S122.
[2] K. Iwashita, M. Oda, Micro-deformation mechanism of shear banding process based on modified distinct element method, Powder Technology 109 (2000) 192–205.
[3] D.A. Horner, J.F. Peters, A.J. Carrillo, Large scale discrete element modeling of vehicle–soil interaction, Journal of Engineering Mechanics 127 (2001) 1027–1032.
[4] P.A. Cundall, A discontinuous future for numerical modeling in soil and rock, in: Discrete Element Methods: Numerical Modeling of Discontinua, Proceedings of the Third International Conference on Discrete Element Methods, ASCE Conference Proceedings 259 (2002) 1, http://dx.doi.org/10.1061/40647(259)1.
[5] S.J. Antony, M.R. Kuhn, Influence of particle shape on granular contact signatures and shear strength: New insights from simulations, International Journal of Solids and Structures 41 (2004) 5863–5870.
[6] L. Rothenburg, N.P. Kruyt, Critical state and evolution of coordination number in simulated granular materials, International Journal of Solids and Structures 41 (2004) 5763–5774.
[7] C. Thornton, L. Zhang, A numerical examination of shear banding and simple shear non-coaxial flow rules, Philosophical Magazine 86 (2006) 3425–3452.
[8] F. Alonso-Marroquin, S. Luding, H.J. Herrmann, I. Vardoulakis, Role of anisotropy in the elastoplastic response of a polygonal packing, Physical Review E 71 (2006) 051304.
[9] C. Salot, P. Gotteland, P. Villard, Influence of relative density on granular materials behavior: DEM simulations of triaxial tests, Granular Matter 11 (2009) 221–236.
[10] T. Matsushima, J. Katagiri, K. Uesugi, A. Tsuchiyama, T. Nakano, 3D shape characterization and image-based DEM simulation of the lunar soil simulant FJS-1, Journal of Aerospace Engineering 22 (2009) 15–23.
[11] P.A. Cundall, O.D.L. Strack, A discrete numerical model for granular assemblies, Geotechnique 29 (1979) 47–65.
[12] M. Oda, K. Iwashita, Mechanics of Granular Materials: An Introduction, A.A. Balkema, Brookfield, VT, 1999.
[13] I. Aranson, L. Tsimring, Granular Patterns, Oxford University Press, 2009.
[14] M. Oda, K. Iwashita (Eds.), Mechanics of Granular Materials: An Introduction, A.A. Balkema, Rotterdam, 1999.
[15] J.S. Andrade Jr., H.J. Herrmann, R.F.S. Andrade, L.R. Da Silva, Apollonian networks: Simultaneously scale-free, small world, Euclidean, space filling and with matching graphs, Physical Review Letters 94 (2005) 018702.
[16] A. Smart, J.M. Ottino, Granular matter and networks: Three related examples, Soft Matter 4 (2008) 2125–2131.
[17] A. Smart, J.M. Ottino, Evolving loop structure in gradually tilted two-dimensional granular packings, Physical Review E 77 (2008) 041307.
[18] A.A. Peña, H.J. Hermann, P.G. Lind, Force chains in sheared granular media of irregular particles, in: M. Nakagawa, S. Luding (Eds.), Powders & Grains 2009, Proceedings of the 6th International Conference Micromechanics of Granular Media 2009, in: AIP Conference Proceedings, vol. 1145, AIP, Colorado, USA, 2009.
[19] D.M. Walker, A. Tordesillas, Topological evolution in dense granular materials: A complex networks perspective, International Journal of Solids and Structures 47 (2010) 624–639.
[20] S.H. Strogatz, Exploring complex networks, Nature 410 (2001) 268–276.
[21] R. Albert, A.-L. Barabási, Statistical mechanics of complex networks, Reviews of Modern Physics 74 (2002) 47–97.
[22] E. Estrada, J.A. Rodríguez-Velázquez, Subgraph centrality in complex networks, Physical Review E 71 (2005) 056103.
[23] E. Estrada, J.A. Rodríguez-Velázquez, Spectral measures of bipartivity in complex networks, Physical Review E 72 (2005) 046105.
[24] P.G. Lind, M.C. González, H.J. Herrmann, Cycles and clustering in bipartite networks, Physical Review E 72 (2005) 056127.
[25] L. da F. Costa, F.A. Rodrigues, G. Travieso, P.R. Villas Boas, Characterization of complex networks: A survey of measurements, Advances in Physics 56 (2007) 167–242.
[26] A. Tordesillas, D.M. Walker, Q. Lin, Force chains and force cycles, Physical Review E 81 (2010) 011302.
[27] A. Tordesillas, Q. Lin, J. Zhang, R.P. Behringer, J.Y. Shi, Structural stability of self-organized cluster conformations in dense granular materials, 2010, in preparation.
[28] A. Tordesillas, D.M. Walker, G. Froyland, R.P. Behringer, J. Zhang, Structural stability and transition dynamics of granular motifs, unpublished manuscript, 2010.
[29] S. Boccaletti, V. Latora, Y. Moreno, M. Chavez, D.-U. Hwang, Complex networks: Structure and dynamics, Physics Reports 424 (2006) 175–308.
[30] A. Drescher, G. de Josselin de Jong, Photoelastic verification of a mechanical model for the flow of a granular material, Journal of the Mechanics and Physics of Solids 20 (1972) 337–340.
[31] A. Tordesillas, J. Zhang, R.P. Behringer, Buckling force chains in dense granular assemblies: Physical and numerical experiments, Geomechanics and Geoengineering 4 (2009) 3–16.
[32] J. Zhang, T.S. Majmudar, A. Tordesillas, R.P. Behringer, Statistical properties of a 2D granular materials subjected to cyclic shear, Granular Matter 12 (2010) 159–172.
[33] F. Radjai, D. Wolf, M. Jean, J. Moreau, Bimodal character of stress transmission in granular packings, Phys. Rev. Lett. 80 (1998) 61–64.
[34] S.N. Dorogovtsev, A.V. Goltsev, J.F.F. Mendes, k-core organization of complex networks, Physical Review Letters 96 (2006) 040601.
[35] A. Tordesillas, Force chain buckling, unjamming transitions and shear banding in dense granular assemblies, Philosophical Magazine 87 (2007) 4987–5016.
[36] M. Muthuswamy, A. Tordesillas, How do interparticle contact friction, packing density and degree of polydispersity affect force propagation in particulate assemblies?, Journal of Statistical Mechanics: Theory and Experiment (2006) P09003.
[37] S.J. Antony, Link between single-particle properties and macroscopic properties in particulate assemblies: Role of structures within structures, Philosophical Transactions of The Royal Society A 365 (2007) 2879–2891.
[38] C. Thornton, L. Zhang, A numerical examination of shear banding and simple shear non-coaxial flow rules, Philosophical Magazine 86 (2006) 3425–3452.
[39] T.-T. Ng, Macro- and micro-behaviors of granular materials under different sample preparations methods and stress paths, International Journal of Solids and Structures 41 (2004) 5871–5884.
[40] M.R. Kuhn, K. Bagi, Contact rolling and deformation in granular media, International Journal of Solids and Structures 41 (2004) 5793–5820.

[41] K. Iwashita, M. Oda, Rolling resistance at contacts in simulation of shear band development by DEM, ASCE Journal of Engineering Mechanics 124 (1998) 285–292.
[42] A. Tordesillas, M. Muthuswamy, On the modeling of confined buckling of force chains, Journal of the Mechanics and Physics of Solids 57 (2009) 706–727.
[43] D. Volfson, L.S. Tsimring, I.S. Aranson, Stick-slip dynamics of a granular layer under shear, Physical Review E 69 (2004) 031302.
[44] F. Dalton, D. Corcoran, Self-organized criticality in a sheared granular stick-slip system, Physical Review E 63 (2001) 061312.
[45] A. Tordesillas, M. Muthuswamy, S.D.C. Walsh, Mesoscale measures of nonaffine deformation in dense granular assemblies, ASCE Journal of Engineering Mechanics 134 (2008) 1095–1113.
[46] R.E. Tarjan, Depth first search and linear graph algorithms, SIAM Journal on Computing 1 (1972) 146–160.